Direct laser-written waveguides for integrated liquid crystal micro-photonics

Igor Muševič *[a,b], Mahendran Vellaichamy[a], Uroš Jagodič[a], Jaka Pišljar[a,b], Andreja Jelen[a], Andriy Nych[c,a], Miha Škarabot[a], Jaka Zaplotnik[b], Miha Ravnik[b,a]

[a]Condensed Matter Department, J. Stefan Institute, Jamova 39, SI-1000 Ljubljana, Slovenia;

[b]Faculty of Mathematics and Physics, University of Ljubljana, Jadranska 19, SI-1000 Ljubljana, Slovenia;

[c] Department of Molecular Photoelectronics, Institute of Physics, Nauky prospect 46, Kyiv, 03680, Ukraine

ABSTRACT

We demonstrate that Direct Laser Writing (DLW) can be used to print low loss planar polymer waveguides on glass, thus promising a novel soft matter platform for polymer all-optic micro-photonics. We printed straight waveguides with various cross sections and lengths up to 900 μm on a 500 nm thin layer of low refractive index CYTOP on glass. We also printed two rectangular micro-prisms at each end of the waveguide, which provides coupling of light in and out of the waveguides. The printed structures were imaged and characterized by SEM and we measured the attenuation of light, propagating along the waveguides. While the high refractive index photosensitive resin IP-n162 shows moderate attenuation of ~14 dB/cm at 580 nm, the IP-S photosensitive resin shows lower attenuation of ~5-9 dB/cm in a rather broad window around 580 nm.

Keywords: liquid crystals, direct laser writing, polymer waveguides, propagation losses

1. INTRODUCTION

Silicon integrated photonics is nowadays mainstream technology that will merge with the existing electronic CMOS integrated circuits to reduce the power consumption in data processing facilities and enhance the data streaming performance within a single integrated circuit. The concepts of silicon technology were developed in a series of investigations of photonic properties of silicon in 1980's[1-5], including early studies of light propagation losses in silicon planar waveguides in the near IR part of the electromagnetic spectrum[1,4]. Silicon integrated photonic platform is compatible with CMOS integrated circuits technology, and is successfully using more than 50 years of engineering development in wafer processing techniques, in particular optical lithography[5-14]. On the other hand, silicon integrated technology has an inherent disadvantage: it is founded on a mature silicon technology, where incremental advancements over the many decades have resulted in steady growth, but is most likely not capable to produce a major technological disruptive breakthrough.

Soft matter, in particular liquid crystals, has the potential for disruptive technological breakthrough in photonics, which was actually demonstrated by the emergence of flat Liquid Crystal Displays (LCDs) in the 1990's. LCDs have not only completely replaced bulky cathode ray tubes in TVs and instrumentation, but have also enabled an extremely great number of novel devices, including portable cell phones that could not be realized using the cathode ray tube technology. Unlike solid state silicon technology that is using high temperatures to process wafers, soft matter is stable near room temperature and must be processed at moderate temperatures. Furthermore, the fluidity and soft nature of soft matter makes it possible to design new materials using simple mixing of different liquids, or dissolving solid materials to dope liquids with optical gain material, using microfluidic flow control and even using the self-assembly properties of soft matter.

Unlike mainstream silicon photonics, research initiatives in soft matter photonics are rather sparse and research efforts are quite limited. Some time ago we demonstrated that liquid crystals could be used as tunable optical micro-resonators[15,16], micro-lasers[17] and optical fibers[18] with excellent wave-guiding properties. It was also demonstrated that self-assembly could be used to bind together different soft matter micro-photonic elements to form a kind of micro-photonic circuitry[19-22]. Because liquid crystals and soft matter are poor conductors of electric current, soft matter photonics is inherently an all-optical platform, where the flow of light is controlled by light.

Liquid Crystals Optics and Photonic Devices, edited by Ibrahim Abdulhalim, Camilla Parmeggiani,
Proc. of SPIE Vol. 13016, 130160H · © 2024 SPIE
0277-786X · doi: 10.1117/12.3022285

We present the first step towards realization of soft matter micro-photonic circuitry, i.e. design, production and characterization of multimode optical waveguides made of polymer that are directly printed on glass using two-photon polymerization technique, known as Direct Laser Writing (DLW) technique. DLW has been extensively used in a number of micro-optical and micro-photonic applications. DLW has been used to produce multimode optical waveguides on glass that were coupled with a light-sensitive optical micro-cavity[23], thus realizing light-tunable optical filter. It has also been demonstrated that DLW patterned surfaces provide an excellent alignment of nematic[24-26], columnar[27], and lyotropic chromonic liquid crystals[28]. An example of a 3D micro-device produced entirely by DLW and using liquid crystals as tunable electro-optic material was also demonstrated recently[29]. Optical properties of the photosensitive resins that are used for two-photon polymerization (TPP) have been studied in considerable detail, both in bulk and printed form[30]. The absorption of light in these materials has been studied in the liquid (non-polymerized) state and after UV curing and thermal treatment. However, there is insufficient knowledge on the propagation losses for polymer micro-waveguides that are printed using the DLW technique.

Here we present our study of propagation of light through multimode optical waveguides that are printed on borosilicate glass covered with a 500 nm thin layer of low refractive index fluoropolymer CYTOP. We printed waveguides using two different resins: (i) The IP-S resin that shows good alignment of NLCs on DLW patterned surfaces[26], but has a refractive index close to glass, (ii) high refractive index resin IP-n162. Waveguides of different length and cross-section have been terminated on both ends with two rectangular prisms. Propagation losses have been measured using the cut-back method (i.e. different lengths of waveguides) by focusing light from a tunable laser onto one of the prisms. The light intensity exiting on the other side of the waveguide was measured using a camera. We present propagation losses for IP-S and IP-n162 waveguides with a cross section of 10μm × 10μm and discuss the accuracy of measuring propagation losses in DLW printed waveguides with two input-output coupling prisms.

2. MATERIALS AND METHODS

We use 3D laser lithography system (Photonic Professional GT+, Nanoscribe GmbH & Co.KG) operating in galvo mode using the 63 × objective that has a printing area of 200 μm. Two different resins were tested, the IP-S resin (Nanoscribe GmbH & Co.KG) with refractive index of 1.486 not polymerized and 1.515 after polymerization, and IP-n162 resin with refractive index of 1.604 in liquid state and 1.622 after polymerization at 589 nm. The waveguides were printed on 22 mm × 22 mm borosilicate glass coverslips (ROTH) of 170±5 μm thickness. The coverslips were first cleaned by hand wiping using lint free cloths and acetone, which was followed by 15 min ultrasound cleaning in 1% water solution of detergent (Hellmanex II) at 35°C. This was followed by 15 min ultrasound cleaning in pure deionized water to remove the traces of detergent. Finally, the slides were dried in an isopropanol degreaser. The coverslips were then spin-coated with fluorinated polymer CYTOP (CTX-809A, Asahi Glass Co., Ltd) that has refractive index of 1.34. A 60:40 % wt solution of CTX-809A and solvent CT-SOLV9AP is spin coated at 1000 RPM onto cleaned substrates and baked at 205°C for 1 hour. This produces a fluoropolymer film of thickness ~ 500 nm that serves as low-refractive index optical isolation layer between borosilicate glass and DLW printed polymer waveguide. CYTOP coated substrates are placed for 5 min into a UVO cleaner (UVO-Cleaner 256-220, Jelight Company, INC.). After 5 min the substrates are blown with nitrogen and a small amount of IPS/IP-n162 resin is drop-casted onto the substrate. A 63× objective NA (Zeiss - 1.4NA Oil Dic, Plan polycromat) is inserted into the printer. The substrates are loaded onto the substrate holder of Nanoscribe and inserted with resin side down into the machine and optical contact is established between the resin and the objective lens. The objective is then carefully moved toward the substrate until the interface of the resin and CYTOP layer is easily found in focus due to the high refractive index mismatch of >0.2. The printing of waveguides is therefore performed in dip-in laser lithography mode (DILL). After printing, the substrates were dipped twice, first for 12 min into PGMEA solvent (Sigma Aldrich), and, second for 1 min in isopropanol. Finally the substrates with printed waveguides and prisms were dried at 40°C for 30 min.

For control purposes, some of printed waveguides were imaged using SEM. The substrates with the printed structures were cut to the appropriate size for imaging and coated with the 10 nm of pure Au. The imaging was performed by Field emission SEM Zeiss SUPRA VP, using secondary electrons (SE) to reveal the topography of the imaged structures. The printed structures were imaged either from top or tilted by 30° to obtain the correlative side view as well.

Propagation losses in printed multimode waveguides were measured using an inverted optical microscope (Nikon Eclipse, TE), a tunable pulsed laser (Opolette HE 355 LD, Opotek, USA) and precision camera (Flir BFS-U3-50S5C). Camera gain and exposure time were kept the same during all experiments to enable quantitative light intensity analysis. Laser

light from the tunable laser system was sent to the microscope objective (ZIESS 20×, NA=0.8 field of view 400 μm) and focused to the input surface of a 45° micro-prism (10 μm × 10 μm footprint). The objective was set to a position to have the exit prism in focus. The intensity pattern of light, exiting on the other 45° micro-prism was monitored with the camera. While monitoring the total intensity of the exiting light, the input beam focus was precisely moved within the x-y plane of the prism surface until maximum of light intensity was reached. The whole procedure was repeated for different lengths *L* of the waveguide. The result was a set of measured light intensities for different waveguides lengths, *I(L).* This set of data was the fitted to an exponentially decaying function of waveguide's length, $I(L) = I_{\circ}e^{-\beta L}$, where β is the propagation loss.

3. RESULTS AND DISCUSSION

Figures 1(a,b) show the CAD model of a waveguide. Each waveguide is designed as a series of single-printed layers that are stacked on each other with a period that is called slicing, as presented in Fig. 1a. In our case we use slicing of 100 nm, which means that neighboring printed layers are strongly overlapping. Namely, the printing voxel has a dimension of ~700 nm along the optical axis of the objective that gives around 600 nm of overlapping of neighboring layers. Individual slices are printed by moving the laser focus along the waveguide, which is followed by displacing the focus for 100 nm perpendicularly to the printed line. Then, subsequent lines are printed along the same direction, which is along the waveguide. The separation between neighboring lines is hatching distance, which is set to 100 nm for all prints. As a final step, contouring is applied, which means that the laser spot is moving along the edges of a printed slice, thereby smoothening the 100 nm finishing polymer layer of the waveguide.

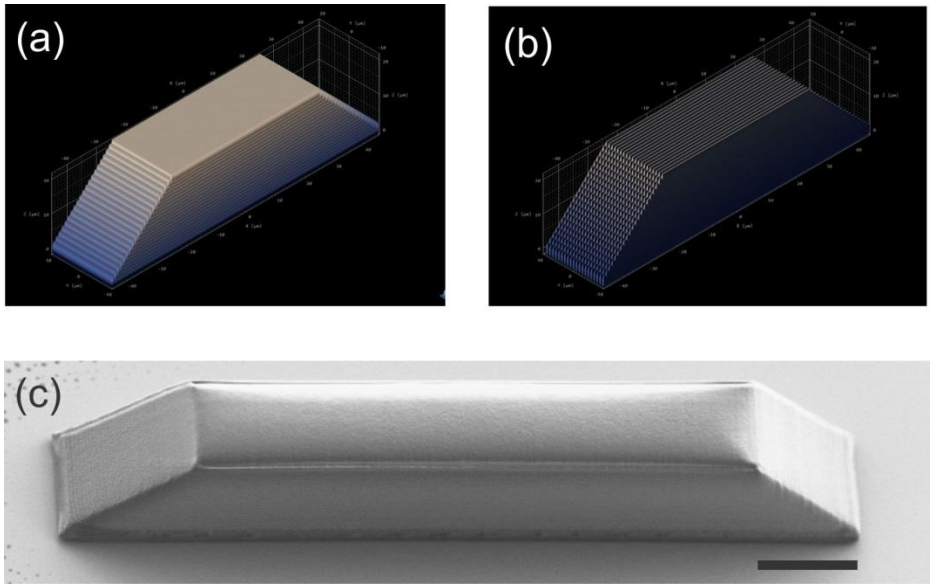

Figure 1. (a) CAD visualization of slicing scheme. The waveguide and prisms are made of a series of slices, stacked on each other with a periodicity of 100 nm, thereby ensuring strong overlapping of printed layers. (b) CAD visualization of printing a selected slice. The focal point is moved in lines along the waveguide, the separation between the lines (hatching distance) is 100 nm. (c) SEM image of 50μm long waveguide with a 10μm × 10 μm cross section made of high refractive index IP-n162 resin. Scale bar is 10 μm. The hatching/slicing distance is 100 nm, number of contours is 2, contour distance is 100 nm, scan speed is set to 1000 and laser power is set to 100% that represents 50 mW. A 63× objective is used in galvo mode of operation.

Figure 1(c) shows SEM image of 50 μm long waveguide with a 10 μm × 10 μm cross section made of high refractive index IP-n162 resin. The surface of the resin looks quite smooth, but more detailed analysis using fluorescent confocal analysis reveals that the structures printed with IP-n162 are quite porous, because it can be infiltrated with fluorescent dye.

The porosity and potential swelling of structures made of IP-n162 is also indicated by the apparently swollen upper surface of the waveguide in Fig. 1(c).

We use optical microscopy to measure the propagation losses in as-printed wavegudes using the cut-back method. The appearance of IP-n162 waveguides under an optical microscope for various wavelengths of measuring light is shown in Figure 2. Figure 3(a) shows the photographs of 580 nm laser beam transmission through 10 μm × 10 μm waveguides on Cytop of different lengths from 10 μm to 170 μm. The measured intensity at the reflected prism for different waveguide lengths is shown in Figure 3(b). At the wavelength of 580 nm (yellow) the transmission losses in IP-n162 waveguides are of the order of ~14 dB/cm.

The propagation losses in IP-n162 DLW printed multimode waveguides are quite high and we explored in more detail the micro-structure of printed waveguides. We exposed printed IP-n162 DLW printed scaffolds to a liquid crystal doped with 0.1% w.t. of fluorescent dye. We used a confocal fluorescence microscope to take 3D images of these samples. We noticed in 3D fluorescent images that after some time the IP-n162 DLW printed scaffolds became fluorescent. This clearly indicates the nanoscale porosity of DLW printed scaffold using IP-n162 resin. In the next step, we repeated the fluorescence test using scaffolds printed with IP-S resin and no diffusion of fluorescent dye was observed into the DLW printed IP-S scaffolds.

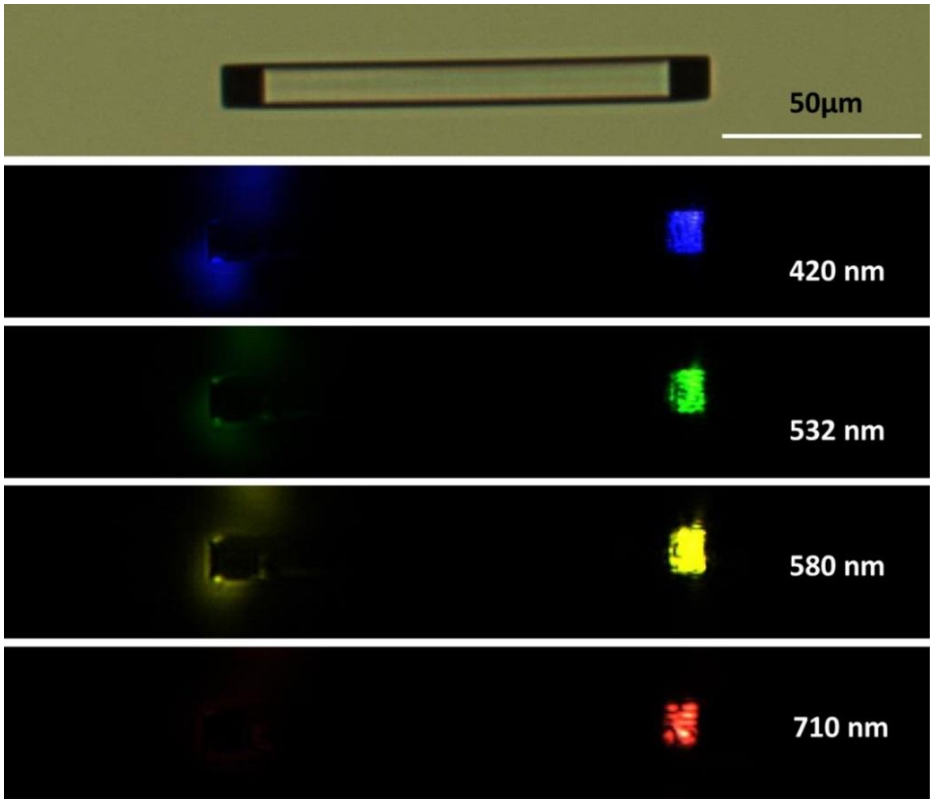

Figure 2. Images of IP-n162 100μm ×10μm ×10μm waveguide (on glass) pumped with different wavelengths from tunable laser, focused through the microscope.

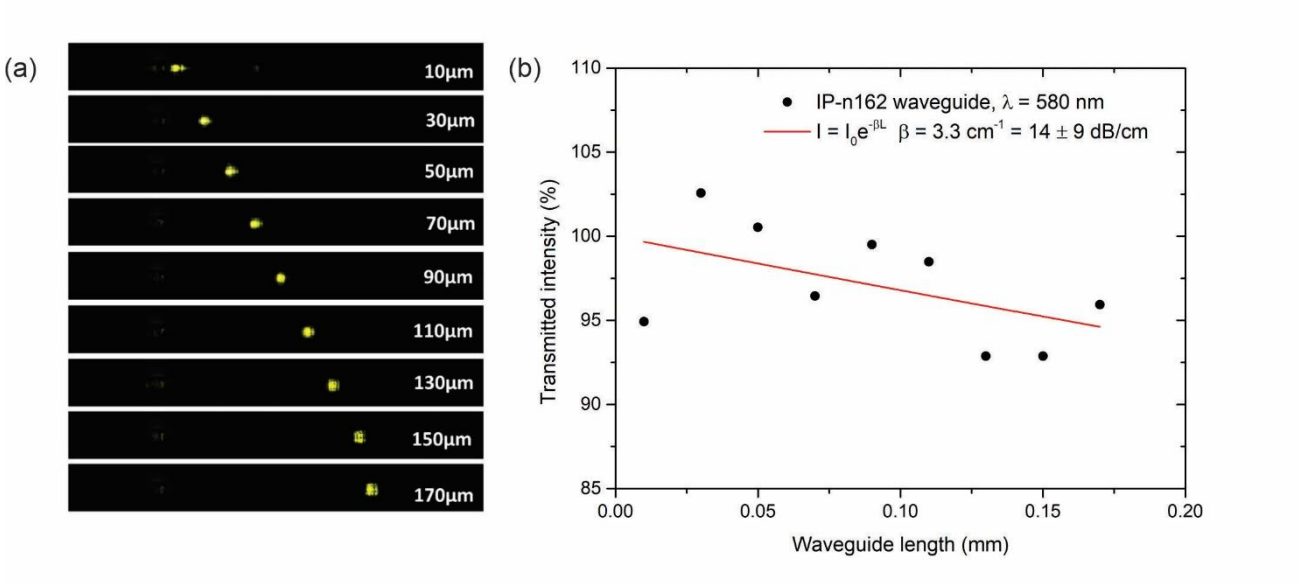

Figure 3. (a) Images of 580 nm laser beam transmission in 10µm ×10µm waveguides (on Cytop) of different lengths. (b) The measured intensity at the reflected prism for different waveguide lengths.

In the next step, we printed IP-S multimode waveguides of 10 µm × 10 µm cross section and variable lengths. By using the stitching function of the Nanoscribe GT printer, we split the waveguides bigger than the print field into individual segments, which are printed separately. This makes it possible to print waveguides up to the maximum 900µm length *L* to increase the accuracy of the measurements of the propagation losses using the cut-back method. Namely, if the propagation losses of waveguides are lower than ~10 dB/cm, the maximum length of ~170 µm of single-print waveguides using the 63× objective results in small attenuation of propagation light at the exit prism, which in turn results in poor accuracy of the measurement of β. This was resolved by increasing the length *L* of DLW printed waveguides up to 900 µm by stitching individual prints. We also performed SEM imaging of IP-S DLW printed waveguides and we found that the surfaces are smooth, the printed IP-S waveguides are not swollen after in contact with fluorescent LC and there are no printing features seen on the surface of IP-S waveguides.

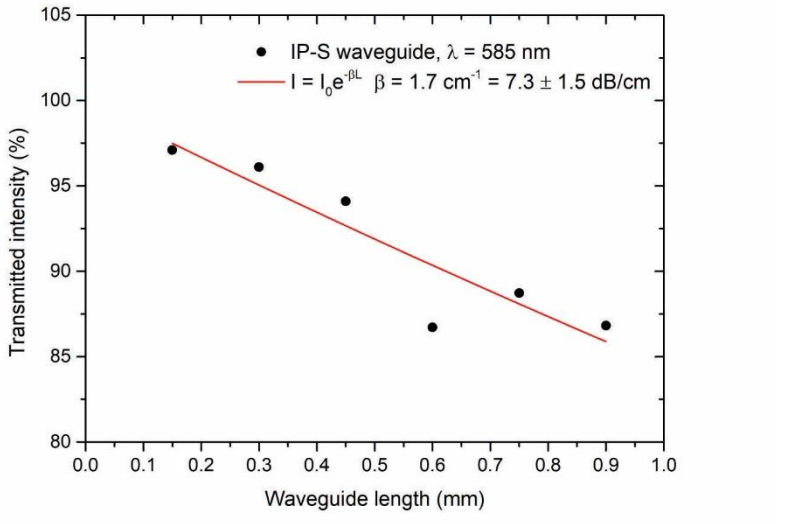

Figure 4. Transmission of 585 nm light propagating through 10µm × 10 µm cross section waveguides printed with IP-S resin on 500 nm CYTOP on glass.

Propagation properties of 585 nm light through 10 μm × 10 μm cross section waveguides printed with IP-S resin on 500 nm CYTOP on glass are shown in Figure 4. The transmission of the printed waveguides is ~90% at the maximum printed length of L=900 μm. This corresponds to propagation losses of 7.3±1.5 dB/cm, which is a reasonably good result for this stage of research. We found that the losses can nearly completely be attributed to the absorption of light in the IP-S resin.

Light propagation through the printed waveguides is also simulated numerically using the finite-difference time-domain (FDTD) method [31] implemented in the MEEP software [32] We perform simulations of light propagation along the lateral cross-section only. Panel (a) of Figure 5 shows the refractive index profile and introduces the geometrical parameters of the structure: the waveguide length L , its height and the prism size, both D . Under the left prism, we place a continuous source shaped as a Gaussian beam with a wavelength of $\lambda = 532$ nm and a waist size of $w_0 = 2.5\ \mu$m with focus at the substrate-waveguide boundary. The polarisation is linear in the z-axis direction. The profile of the z-component of the electric field $E_z(x, y)$ in a waveguide of length $L = 40\ \mu$m and thickness $D = 5\ \mu$m is shown in panel (b). At the entrance prism, light undergoes total internal reflection which provides coupling into the waveguide, but some light still escapes at and around the corners. At the planes labelled *IN*, *1*, ... , *9*, *OUT*, we measure the Poynting flux of light in the direction of propagation, i.e. on the *IN* plane along $\hat{\mathbf{e}}_y$, on the 1, ... , 9 planes in the $\hat{\mathbf{e}}_x$ direction and on the *OUT* plane in the $-\hat{\mathbf{e}}_y$ direction. As shown in the inset of panel (b), light is mostly lost at the first prism, the flux is then approximately constant along the waveguide, and finally, part of the light energy is lost at the exit prism as well.

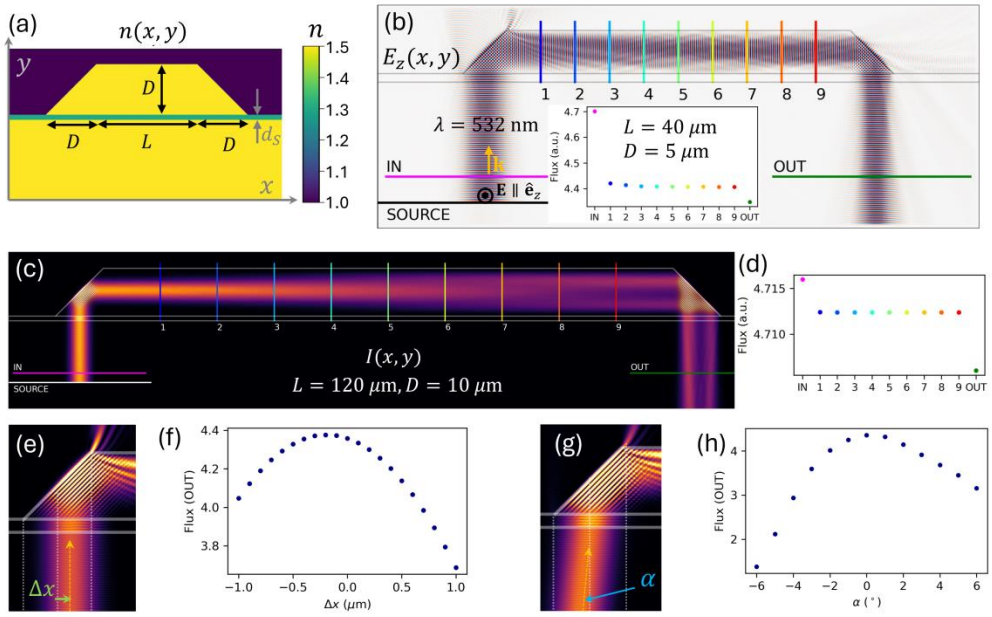

Figure 5. (a) Refractive index profile $n(x, y)$ of the studied structure. (b) Electric field $E_z(x, y)$ in a waveguide of thickness $D = 5\ \mu$m and length $L = 40\ \mu$m with Poynting flux measured at selected planes *IN, 1, ..., 9, OUT* along the beam in the inset. (c) Light intensity profile $I(x, y)$ in a waveguide of thickness $D = 10\ \mu$m and length $L = 120\ \mu$m. (d) Poynting flux at planes *IN, 1, ..., 9, OUT*, as indicated in panel (c). (e) Displacement of the incoming beam Δx. (f) Poynting flux measured at the *OUT* plane under a waveguide of thickness $D = 5\ \mu$m and length $L = 120\ \mu$m for varying Δx. (g) Angle α between the incoming beam direction and the normal to the substrate-waveguide interface. (h) Poynting flux measured at the *OUT* plane under a waveguide of thickness $D = 5\ \mu$m and length $L = 120\ \mu$m for varying incoming angle α.

For a constant beam waist $w_0 = 2.5\ \mu$m, total losses, measured as a ratio between Poynting fluxes measured at *IN* and *OUT* planes, decrease with increasing D (entrance prism size and waveguide thickness). In a waveguide with $D = 10\ \mu$m, the relative loss of light energy is even greater at the exit prism than at the entrance prism, as shown in panels (c,d) of Figure 5. The reason is that the beam at the entrance prism is much narrower than the size of the prism, but on the way to the exit prism, it becomes wider and already extends to the sharp corners, where the losses are significant.

The experimental measurement of the waveguide attenuation is sensitive to the illumination setup, since the measured output flux (at the *OUT* plane) varies greatly with: (1.) the displacement of the incoming beam with respect to the centre of the prism Δx, and (2.) the incident angle α, defined as the angle between the direction of beam propagation and the normal to the substrate-waveguide interface. The change of the flux at the *OUT* plane due to the variation of Δx and α is demonstrated in panels (e–h) of Figure 5. For example, a displacement of the beam with waist size $w_0 = 2.5\ \mu$m at the prism of the waveguide of thickness $D = 5\ \mu$m for $\Delta x = 0.5\ \mu$m to the right results in a decrease of the measured flux already by 5%. Interestingly, it is not optimal to target the centre of the prism since the maximum flux at the *OUT* plane is measured if the beam is shifted by $\Delta x = -0.2\ \mu$m to the left. Even more than the displacement of the beam, the measured flux is affected by the angle of incidence α. For given refractive indices ($n_P = 1.5$ for the prism and $n = 1.0$ for surrounding air), the limiting angle for total internal reflection is $\beta_c \approx 41.8°$. For a normal beam incidence ($\alpha = 0°$), the angle of incidence at the prism surface is $\beta = 45°$, which satisfies the condition for total internal reflection, but a tilt of the beam α by just a few degrees in negative direction causes the reflection on the entrance prism to be no longer perfect. Alternatively, the angle of incidence to the surface of the entrance prism can be increased in positive direction, but the consequence is a decreased flux of the beam at the *OUT* plane due to the imperfect reflection at the exit prism. Overall, as shown in panel (h), the orthogonal incidence ($\alpha = 0°$) is optimal. For example, tilting the beam by $\alpha = -3°$ decreases the flux at the *OUT* plane by almost 20%.

4. CONCLUSIONS

We demonstrate that 2-photon DLW technique can be used to print low-loss polymer waveguides on glass with optical isolation. For waveguides that were DLW printed using the IP-S resin, the losses at 550 nm are of the order of ~5 dB/cm, which means that only ~10% of light is lost in a millimeter-long waveguide. This means that for research purposes the IP-S and IP-n162 waveguides are excellent. We anticipate that propagation losses are even lower in the red and near IR part of the spectrum. However, propagation losses lower than 1dB/cm are difficult to measure using the micro-prism couplers, which means that new methods need to be designed or the existing method has to be refined. Nevertheless, the DLW printing of more complex polymer photonic circuits seems to be a promising direction.

ACKNOWLEDGEMENTS

This result is part of a project that has received funding from the European Research Council (ERC) under the European Union's Horizon 2020 research and innovation program (Grant agreement No. 884928-LOGOS).

REFERENCES

[1] Soref, R. A., and Lorenzo, J. P., "All-Silicon Active and Passive Guided-Wave Components for λ= 1.3 and 1.6 μm," *IEEE J. Quant. Electr.* QE-**22**(6), 873-879(1986).

[2] Lorenzo, J. P. and Soref, R. A., "1.3 μm electro-optic silicon switch", *Appl. Phys. Lett.*, **51**(1), 6-8(1987).

[3] Soref, R. A., Bennett, B. R., " Electrooptical Effects in Silicon", *IEEE J. Quant. Elect.*, QE-**23**(1), 123-129(1987).

[4] Weiss, B. L ., Reed, G. T., Toh, S. K., Soref, R. A. and Namavar, F., "Optical Waveguides in SIMOX Structures", *IEEE Photon. Tech. Lett.* **3**(1), 19-21(1991).

[5] Little, B. E., Foresi, J. S., Steinmeyer, G., Thoen, E. R., Chu, S. T., Haus, H. A., Ippen, E. P., Kimerling, L. C., Greene, W., " Ultra-Compact Si–SiO Microring Resonator Optical Channel Dropping Filters", *IEEE Photon. Tech. Lett.*, **10**(4), 549-551(1998).

[6] Taillaert, D., Bogaerts, W., Bienstman, P., Krauss, T. F., Van Daele, P., Moerman, I., Verstuyft, S., De Mesel, K., Baets, R., " An Out-of-Plane Grating Coupler for Efficient Butt-Coupling Between Compact Planar Waveguides and Single-Mode Fibers", *IEEE J. Quant. Elect.*, **38**(7), 949-955(2002).
[7] Almeida, V. R., Panepucci, R. R., Lipson, M., " Nanotaper for compact mode conversion", *Opt. Lett.*, **28**(15), 1302-1304(2003).
[8] Almeida, V. R., Barrios, C. A., Panepucci, R. R., Lipson, M., " All-optical control of light on a silicon chip", *Nature*, **431**(28 October 2004), 1081-1084(2004).
[9] Dumon, P., Bogaerts, W., Wiaux, V., Wouters, J., Beckx, S., Van Campenhout, J., Taillert, D., Luyssaert, B., Bienstman, P., Van Thourhout, D., Baets, R., " Low-Loss SOI Photonic Wires and Ring Resonators Fabricated With Deep UV Lithography", *IEEE Photon. Tech. Lett.*, **16**(5), 1328-1330(2004).
[10] Liu, A., Jones, R., Liao, L., Samara-Rubio, D., Rubin, D., Cohen, O., Nicolaescu, R., Paniccia, M., " A high-speed silicon optical modulator based on a metal–oxide–semiconductor capacitor", *Nature*, **427**(12 February 2004), 615-618(2004).
[11] Bogaerts, W., Baets, R., Dumon, P., Wiaux, V., Taillaert, D., Luyssaert, B., Van Campenhout, J., Bienstman, P., Van Thourhout. D., " Nanophotonic Waveguides in Silicon-on-Insulator Fabricated With CMOS Technology", *J. Lightwave Tech.* **23**(1), 401-412(2005).
[12] Rojo Romeo, P., Van Campenhout, J., Regreny, P., Kazmierczak, A., Seassal, C., Letartre, X. Hollinger, G., Van Thourhout, D., Baets, R., Fedeli, J.M., Di Cioccio, L., " Heterogeneous integration of electrically driven microdisk based laser sources for optical interconnects and photonic ICs", *Opt. Exp*. **14**(9), 3864-3871(2006).
[13] Chang, Hsu-Hao, Fang, A. W., Sysak, M. N., Park, H., Jones, R., Cohen, O., Raday, O., Paniccia, M. J., and Bowers, J. E., " 1310 nm silicon evanescent laser", *Opt. Exp.* **15**(18), 11466-1147(2007).
[14] Lipson, M., "The revolution of silicon photonics", *Nature Materials*, **21**(September 2022), 974-975(2022).
[15] Humar, M., Ravnik, m. Pajk, S., and Muševič, I., "Electrically tunable liquid crystal optical microresonators," *Nat. Photonics* **3**, 595-600 (2009).
[16] Humar, M. and Muševič, I., "Surfactant sensing based on whispering-gallery-mode lasing in liquid-crystal microdroplets", *Optics Express* **19**, 19836-19844(2011).
[17] Humar, M., and Muševič, I., "3D microlasers from self-assembled cholesteric liquid-crystal microdroplets," *Opt. Express* **18**, 26995–27003 (2010).
[18] Peddireddy, K., Jampani, V. S. R., Thutupalli, S., Herminghaus, S., Bahr, Ch. and Muševič, I., "Lasing and waveguiding in smectic A liquid crystal optical fibers," *Optics Express* **21**, 30233-30242 (2013).
[19] Musevic, I., "Nematic colloids, topology and photonics", *Phil. Trans. Royal Soc. A* **371**, 20120266 DOI: 10.1098/rsta.2012.0266 (2013).
[20] Musevic, I., Skarabot, M., Humar, M., "Direct and inverted nematic dispersions for soft matter photonics", *J. Phys. Cond. Matter* **23**(28), 284112-1-284112-7 (2011).
[21] Coles, H. and Morris, S. 2010 Liquid-crystal lasers. Nature Photonics 4,676–685.
[22] Cipparrone, G., Mazzulla, A., Pane, A., Hernandez, R. J., Bartolino, R. 2011 Chiral self-assembled solid microspheres: A novel multifunctional microphotonic device. *Adv. Mat.* **23**, 5773-5778.
[23] Nocentini, S., Riboli, F., Burresi, M., Martella, D., Parmeggiani, C., and Wiersma, D. S., "Three-Dimensional Photonic Circuits in Rigid and Soft Polymers Tunable by Light", *ACS Photonics*, **5**, 3222-3230(2018).
[24] Lee, Chee Heng, Yoshida, H., Miura, Y., Fujii, A., and Ozaki, M., "Local liquid crystal alignment on patterned micrograting structures photofabricated by two photon excitation direct laser writing" *Appl. Phys. Lett.* **93**, 173509(2008).
[25] Zhang, B., Plidschun, M., Schmidt, M. A., Kitzerow, H.-S., "Anchoring and electro-optic switching of liquid crystals on nano-structured surfaces fabricated by two-photon based nano-printing", *Opt. Mat. Express*, **13**(12), 3467-3480(2023).
[26] Jagodič, U., Vellaichammy, M., Škarabot, M., Muševič, I., "Surface alignment of nematic liquid crystals by direct laser writing of photopolymer alignment layers", *Liq. Cryst.* (2023), DOI: 10.1080/02678292.2023.2242297.
[27] Tokuoka, K., Yoshida, H., Miyake, Y., Lee, C. H., Miura, Y., Suzuki, S., Fujii, A., Shimizu, Y., and Ozaki, M., "Planar Alignment of Columnar Liquid Crystals in Microgroove Structures", *Mol. Cryst. Liq. Cryst.* **510**, 1260-1267(2009).
[28] Guo, Y., Shahsavan, H., Davidson,Z. S., and Sitti, M., "Precise Control of Lyotropic Chromonic Liquid Crystal Alignment through Surface Topography", *ACS Appl. Mat. Interf.* **11**, 36110-36117(2019).
[29] He, Z., Tan, G., Chanda, D., Wu, S.-T., "Novel liquid crystal photonic devices enabled by two-photon polymerization", *Opt. Exp.* **27**(8), 11472-11491(2019).

[30] Hasan, M., Blair, S., "Maximizing transmittance in two-photon 3D printed materials for micro-optics in the visible", *Opt. Mat. Express* **12**(3), 895-906(2022).
[31] Taflove, A., Oskooi, A., and Johnson, S. G., [*Advances in FDTD computational electrodynamics: photonicsand nanotechnology*], Artech house (2013).
[32] Oskooi, A. F., Roundy, D., Ibanescu, M., Bermel, P., Joannopoulos, J. D., and Johnson, S. G., "Meep: A flexible free-software package for electromagnetic simulations by the fdtd method," *Computer Physics Communications* **181**(3), 687–702 (2010).